RSC Advances

This is an *Accepted Manuscript*, which has been through the Royal Society of Chemistry peer review process and has been accepted for publication.

Accepted Manuscripts are published online shortly after acceptance, before technical editing, formatting and proof reading. Using this free service, authors can make their results available to the community, in citable form, before we publish the edited article. This *Accepted Manuscript* will be replaced by the edited, formatted and paginated article as soon as this is available.

You can find more information about *Accepted Manuscripts* in the **Information for Authors**.

Table of contents entry

A new ^{99m}Tc-labeled bivalent DTPA-bis-c(RGDfK) conjugate has been developped and succesfully synthesized. Promising results have been obtained for its preclinical evaluation on human glioma and melanoma tumor expressing $\alpha_v\beta_3$ targets.

Keywords: SPECT imaging, integrin $\alpha_v\beta_3$, ^{99m}Tc-DTPA-bis-c(RGDfK), melanoma, glioma, neoangiogenesis.
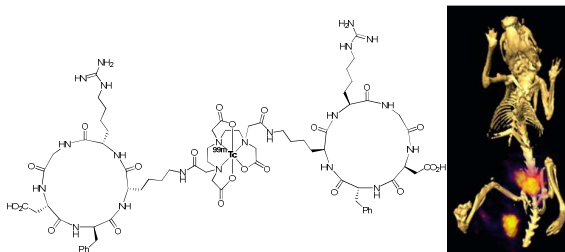
^{99m}Tc-DTPA-bis-c(RGDfK) a potential alpha(v)beta3 integrin based homobivalent radioligand for imaging neoangiogenesis in malignant glioma and melanoma

Frédéric Debordeaux,*[ab] Jürgen Schulz,[ab] Catherine Savona-Baron,[ab] Puja Panwar Hazari,[c] Cyril Lervat,[ab] Anil Kumar Mishra,[c] Colette Ries,[ab] Nicole Barthe,[ef] Béatrice Vergier,[d] and Philippe Fernandez[ab]

$\alpha_v\beta_3$ integrin is a marker of tumor neoangiogenesis that specifically binds to RGD containing peptides. Hence, the present study is focused on the development of ^{99m}Tc-labeled bivalent DTPA-bis-c(RGDfK) conjugate and its preclinical evaluation on human tumor cell lines expressing $\alpha_v\beta_3$ targets. Homobivalent DTPA-bis-c(RGDfK) was prepared and assessed for its affinity and specificity in $\alpha_v\beta_3$ positive (and negative) receptor cell lines. DTPA-bis-c(RGDfK) conjugate was labeled with ^{99m}Tc and subjected to cells/tissue sections. Localization of $\alpha_v\beta_3$ expression was corroborated using immunostaining and *ex vivo* imaging of the distribution pattern of ^{99m}Tc-DTPA-bis-c(RGDfK). The radiolabeling of the DTPA-bis-c(RGDfK) with ^{99m} is obtained after 45 min at 95°C with a radiochemical yield of about 45%. Radiochemical purity was > 95% after C18 Oasis HLB cartridge purification with specific activity of 1475 GBq/mmoL. *In vitro* experiments showed high affinity and specificity for $\alpha_v\beta_3$ with IC_{50} of 32.86 ± 7.83 nmol/L. *Ex vivo* imaging on tissue sections confirmed preliminary specificity results. *In vivo* analysis in mouse model showed that this tracer was able to detect and readily identify U87MG and B16F10 $\alpha_v\beta_3$ positive tumors 60 minutes post-injection. c(RGDfK) blocking experiments confirmed its excellent affinity and specificity to $\alpha_v\beta_3$ receptors in U87MG tumors. The radiotracer was mainly excreted through the renal route with minimal radioactivity being excreted through hepatobiliary route. ^{99m}Tc-DTPA-bis-c(RGDfK) can be an excellent scintigraphic agent for imaging of $\alpha_v\beta_3$ receptors being expressed in abundance in malignant glioma and melanoma cancer.

Introduction

Angiogenesis is a key requirement to provide oxygen and nutrients for both metastasis and tumor growth. Tumor neoangiogenesis is a predictive element of the evolution of numerous cancers.[1,2] So, the development of antiangiogenic therapeutic reinforces the interest for the imaging of neoangiogenesis. Integrins are heterodimeric transmembrane glycoproteins consisting of non-covalently associated α and β subunits, possessing the sequence Arginine-Glycine-Aspartic acid (RGD) through a specific recognition and playing an important role in the regulation of various intracellular signalling pathways.[3] Among them, the integrin $\alpha_v\beta_3$ is highly expressed in tumors such as osteosarcomas, neuroblastomas, glioblastomas, malignant melanomas, breast, lung and prostate carcinomas but its expression is weak in most healthy organ systems. Moreover, multivalency or dimerization increases the interaction during receptor clustering after initial monovalent binding is initiated. The multivalency effect has been established previously using dimeric and tetrameric RGD peptides to enhance tumor targeting efficacy and to obtain better *in vivo* imaging results.[4]

Despite aggressive therapeutics with surgery, radiotherapy and chemotherapy, malignant gliomas remain more often fatal. Malignant glioma is among the most highly vascular of human tumors. Microvascular density is an independent prognostic factor for adult gliomas and angiogenesis represents an especially attractive target for their treatment.

For melanomas, early detection is crucial for prognosis. Anatomical imaging seems limited for precise therapeutic answer. The pattern of melanoma is often unpredictable, and conventional imaging provides limited value for accurate staging and quantification of the disease burden. Given these limitations, a new imaging tool allowing the early diagnosis of metastatic disease either at the level of nodal or distant organs seems essential.

[a.] Univ. Bordeaux, INCIA, UMR 5287, F-33400 Talence, France

[b.] CNRS, INCIA, UMR 5287, F-33400 Talence, France

[c.] Division of Cyclotron and Radiopharmaceutical Sciences, Institute of Nuclear Medicine and Allied Sciences, DRDO, New Delhi, India 110052

[d.] CHU de Bordeaux, Service d'anatompathologie, F-33000 Bordeaux, France

[e.] Univ. Bordeaux, Bioingénierie tissulaire, U1026, F-33000 Bordeaux, France

[f.] INSERM, Bioingénierie tissulaire, U1026, F-33000 Bordeaux, France

† Electronic Supplementary Information (ESI) available. See DOI: 10.1039/x0xx00000x
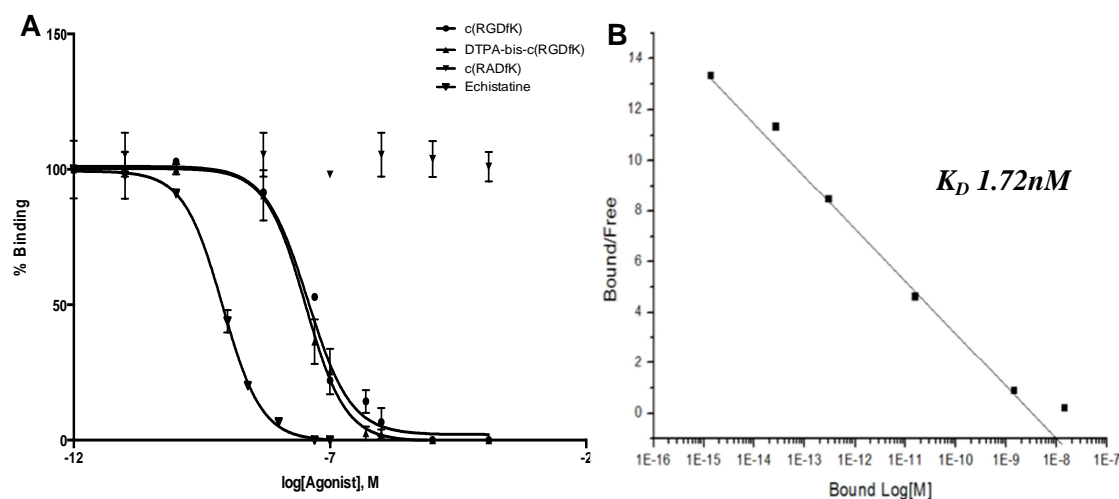
Fig 1. (A) Displacement experiments using increasing concentrations of unlabeled DTPA-bis-c(RGDfK). Each point was the average of triplicate data points and the results shown were representative of three experiments. The best IC_{50} value was obtained for echistatin with 0.79 ± 0.29 nmol/L. The IC_{50} results were 32.86 ± 7.83 nmol/L, and 46.83 ± 14.74 nmol/L for DTPA-bis-c(RGDfK), and c(RGDfK) respectively. c(RADfK) was used as negative control. **(B)** Binding assays on U87MG cells using increasing concentrations of ^{99m}Tc-DTPA-bis-c(RGDfK). The Kd results were 1.72 ± 0.12 nmol/L for ^{99m}Tc-DTPA-bis-c(RGDfK).

It has been proven that cyclization of the RGD sequence not only results in increased selectivity and affinity with better targeting capability, but also in higher cellular uptake through the integrin dependent endocytosis pathway and better resistance to the action of serum proteases. As dimeric peptides offered good tumor selectivity and good T/B ratios,[5–10] and as DTPA (Diethylene Triamine Penta acetic Acid) showed excellent complexation results with ^{99m}Tc for medical imaging, a new dimeric ^{99m}Tc-DTPA-bis-c(RGDfK) tracer has been developed in our laboratory.

The objective of this study is to establish a new bifunctional dimeric c(RGDfK) probe to evaluate neoangiogenesis in glioma and melanoma cell lines using *ex vivo* and *in vivo* imaging. ^{99m}Tc-DTPA-bis-c(RGDfK) structure presents a chelator, which is necessary for ^{99m}Tc-labeling and two cyclic RGD peptide motifs in order to contribute to multiple binding and high local concentration of the tracer at target site. We intend to exemplify this ^{99m}Tc tracer on highly neovascularized tumoral models: malignant melanoma and glioma for which angiogenesis is fundamental in tumor growth, invasiveness and metastasis.

Results

Solid-phase receptor binding assay

This assay helped us to estimate the value of inhibitory concentration 50 (IC_{50}). Radiolabeled echistatin was added to the cells in the presence of competitors. Non-specific binding was determined in presence of an excess of echistatin (1000 fold molar excess). Each point was the average of triplicate data points and the results were representative of three experiments (Fig. 1A).

The labeled peptide and positive controls inhibited the binding of ^{125}I-Echistatin to $\alpha_v\beta_3$ integrin in a dose-dependent manner. The IC_{50} values obtained for echistatin, DTPA-bis-c(RGDfK), and

c(RGDfK) were respectively 0.79 ± 0.29 nmol/L, 32.86 ± 7.83 nmol/L, and 46.83 ± 14.74 nmol/L. Competition experiments with c(RADfK) showed no inhibition of ^{125}I-Echistatin binding even at the highest concentration tested. ^{99m}Tc-DTPA-bis-c(RGDfK) displayed high affinity for the $\alpha_v\beta_3$ receptors. Cell binding assays on U87MG was also performed. Kd value was 1.72 ± 0.12 nmol/L and confirmed the high affinity of the tracer for $\alpha_v\beta_3$ integrin (Fig. 1B).

Immunocytochemical, cytotoxicity and immunohistochemical analysis

Immunocytochemical studies were performed to characterize the $\alpha_v\beta_3$ expression on the cell lines used in the present study. Non-specific binding has been evaluated in similar conditions but without the use of the primary antibody LM609. C6 cells were also confirmed as negative control, and U87MG as positive one with numerous membrane binding.

SKMEL28 cells presented lots of membranous clusters in particular in expansion area testifying the presence of the integrin $\alpha_v\beta_3$ in the plates of anchoring.

Fluorescent heap specific for $\alpha_v\beta_3$ was identified for B16F10 cells (data not shown).

Integrin expression of our cells was confirmed by flow cytometric analysis in a Becton Dickinson FACSCanto II flow cytometer (San Jose, California).

DTPA-bis-c(RGDfK) was evaluated for its ability to induce cytotoxicity on the U87MG and HEK cell lines using a methylthiazole tetrazolium (MTT) assay (see supplementary information for experimental procedure).

The cells exposed to DTPA-bispharmacophore conjugate showed concentration-dependent cell death that was statistically significant above 1 mM. The IC_{50} values of the tracer were 0.81 ± 0.03 mM for U87MG cells (data not shown) and 1.02 ± 0.03 mM for HEK cells (Fig. S1 in supplementary information).
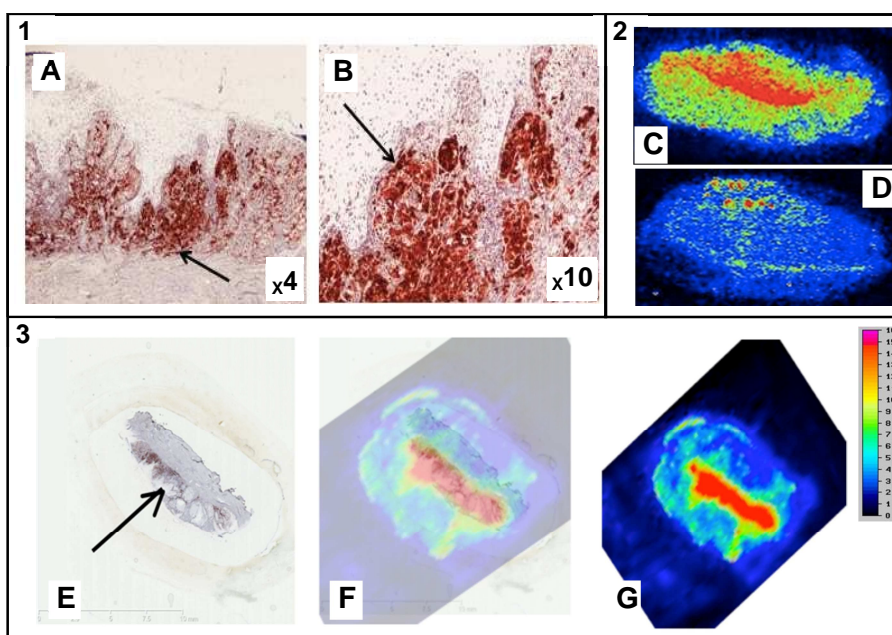
Fig. 2 1(A) Immunostaining using anti-$\alpha_v\beta_3$ human murine monoclonal antibody (LM609). Localization of high integrin expression in SS melanoma (red color) and **(B)** zoom of SS melanoma immunostaining. **2(C)** Radiolabeling of tissue section of SS melanoma with ^{99m}Tc-DTPA-bis-c(RGDfK), **(D)** displacement study of ^{99m}Tc-DTPA-bis-c(RGDfK) on tissue sections of SS melanoma in the presence of an excess of cold ligand c(RGDfK). **3** Comparison of the results obtained by radiolabeling with ^{99m}Tc-DTPA-bis-c(RGDfK) and by immunostaining. **(E)** Immunostaining of SS melanoma using anti-$\alpha_v\beta_3$ human murine monoclonal antibody (LM609). **(F)** Merged Images. **(G)** Radiolabeling with ^{99m}Tc-DTPA-bis-c(RGDfK).

The tested concentration of the radiolabeled conjugate was 0.68 µM and hence with an IC_{50} value of 1.02 mM, the synthesized conjugate can be considered as a nontoxic and safe diagnostic agent.

Different tissues were tested concerning the expression of the integrin $\alpha_v\beta_3$. Naevus, and healthy brain, $\alpha_v\beta_3$ negative controls, did not show binding of the antibody LM609, which indicated the absence of overexpression of the integrin $\alpha_v\beta_3$. Superficial Spreading melanoma (SS melanoma), $\alpha_v\beta_3$ positive tumor, showed an important uptake at the level of junction area between dermis and epidermis (Fig. 2). Considering brain tumors, the expression of $\alpha_v\beta_3$ seemed to increase with the grade of the tumor. Localization, which was restricted in endothelial cells for low-grade tumors (Fig. 3C), was more largely present for high-grade tumor with both endothelial cells and tumor cells expressions (Fig. 3D,E).
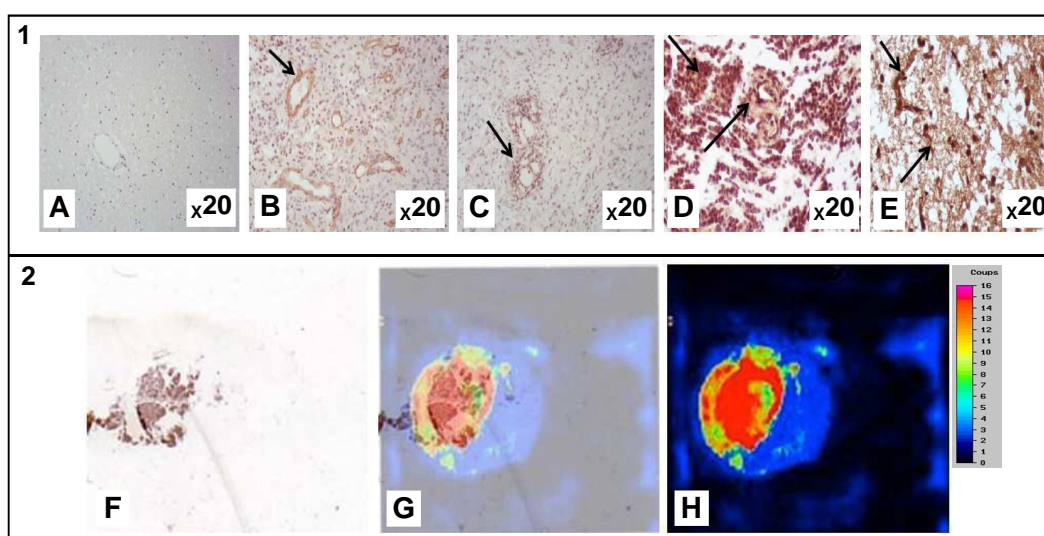
Fig. 3 1(A) Immunostaining using anti-$\alpha_v\beta_3$ human murine monoclonal antibody (LM609). Localization of high integrin expression in respectively **(A)** negative control (healthy brain), **(B)** adult glioblastoma, **(C)** pilocytic astrocytoma of the child, **(D)** anaplastic astrocytoma of the child and **(E)** glioblastoma of the child. **2** Comparison of the results obtained by radiolabeling with ^{99m}Tc-DTPA-bis-c(RGDfK) and by immunostaining of anaplastic astrocytoma. **(F)** Immunostaining of anaplastic astrocytoma with anti-$\alpha_v\beta_3$ human murine monoclonal antibody (LM609). **(G)** Merged Images. **(H)** Radiolabeling with ^{99m}Tc-DTPA-bis-c(RGDfK).

99mTc labeling, purification, log *P* and stability

The initial radiochemical yield was optimized and the desired radiolabeling of DTPA-bis-c(RGDfK) with ^{99m}Tc was realized. Various quantities and different reducing agent were tested and the best results were obtained when 390 µg of precursor DTPA-bis-c(RGDfK) and 50 µg of $SnCl_2$ as reducing agent were used.

The radiochemical purity was > 95% with specific activity of 1475 GBq/mmoL, and the non-decay corrected radiochemical yield was about 45% (n = 10). HPLC results showed a retention time for the ^{99m}Tc-DTPA-bis-c(RGDfK) of 6.2 min. Reduced technetium was the main radiochemical impurity.

^{99m}Tc-DTPA-bis-c(RGDfK) presented hydrophilic properties characterized by a log *P* value of -1.78 (n = 3).

Stability studies under *in vitro* conditions revealed the high stability of the complex prepared. The radiochemical purity was unchanged over a period of 3 hours (0, 30, 60, 120 and 180 min) and the percentage of remaining ^{99m}Tc-DTPA-bis-c(RGDfK) was calculated with a mean value of 95 ± 3.0%. No significant release of technetium or peptide degradation was observed over a 3 h period.

Time course and kinetics of transport of ^{99m}Tc-DTPA-bis-c(RGDfK)

At first, the binding ability of the radiotracer was estimated on four cell lines (C6, B16F10, SKMEL28, U87MG).

The cell binding studies were carried out as a function of peptide concentrations and incubation times. The radiolabeled peptide radioactivity of 1.0 MBq/mL used in the present study provided a reasonable balance between the cell binding and background signal. The variance analysis (ANOVA test) of the results for the different cell lines showed a significant difference (p<0.0001) for time and time/concentration parameters. A significant difference (p<0.05) was also observed according to the time/cell line type parameter.

The binding of the tracer underlined the existence of a plateau, which can be obtained after 90 min of incubation for both melanoma and glioma cells (Fig. S2 in supplementary information).

Radiolabeling of tumor tissue sections

The radiolabeling of the slices of melanoma and glioma tended to confirm the results previously obtained in immunostaining. Micro-imager analysis showed an adequacy with the interaction of the LM609 monoclonal antibody. The merger of the obtained images revealed a good co-localization on samples of SS melanoma and anaplastic astrocytoma between the binding of the anti-$\alpha_v\beta_3$ antibody and the labeling of the tracer. Displacement study realized on glioma and melanoma confirmed previous results with a very low signal of the radiotracer (Fig. 2, 3).

SPECT-CT imaging of tumor bearing mice

The figure 4 illustrates the selected SPECT-CT (Single Photon Emission Computed Tomography) images of tumor bearing mice administered with 18.5 MBq of ^{99m}Tc-DTPA-bis-c(RGDfK), at 30 min post-injection. ^{99m}Tc-DTPA-bis-c(RGDfK) injected to the animal allowed localization of the U87MG tumor used here as a positive control of the expression of the integrin $\alpha_v\beta_3$ and grafted at the level of the right posterior leg of the animal (Fig. 4B).
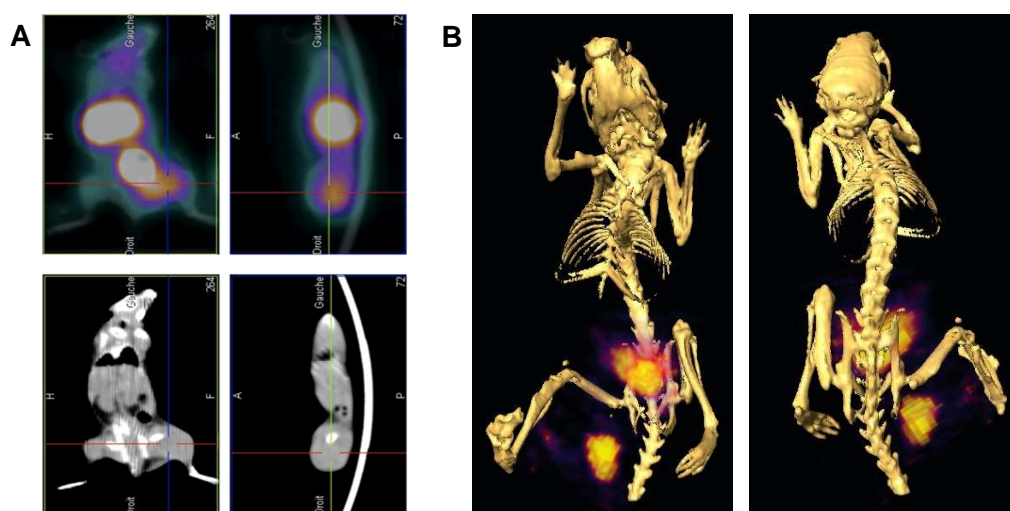
Fig. 4 Administration of the ^{99m}Tc-DTPA-bis-c(RGDfK) activity in nude xenografted mouse, SPECT-CT coronal and transaxial images, 30 min p.i. **(A)** The tracer was injected in nude mice (n = 6) each possessing a different tumoral type xenografted on posterior legs. The injection of the ^{99m}Tc radiolabeled peptide allowed the localization of the B16F10 tumor on the right leg. A clearly hot spot was observed compared to the background. Additional high activity was found in the bladder and kidney indicating predominant renal excretion. **(B)** Anterior and posterior views from reconstructed images of mice bearing U87MG $\alpha_v\beta_3$-positive tumor. It was possible to clearly identify the tumor and an important renal excretion pathway.

The left leg carrying the C6 tumor, negative control of the expression of the integrin $\alpha_v\beta_3$, did not show viewable binding of the tracer. The reconstructed images obtained with FLEX SPECT TM confirmed readily observation of $\alpha_v\beta_3$ positive tumor on right posterior leg of another animal. The third mouse was characterized by the presence of melanocytic tumor B16F10 on posterior leg (Fig. 4A). A good binding of the radiotracer was observed and tumors stood out with a good contrast compared with surrounding tissues. Receptor specificity was confirmed by blocking experiments.

For the c(RGDfK) blocking experiments, mice bearing U87MG tumors were scanned (15 min tomography) after the injection of 24.2 MBq with 1 h block using ~300 fold excess of native c(RGDfK) (101.7 µg/kg/mice). 97.88 % block was observed confirming the receptor specificity at the target site (Fig. 5).
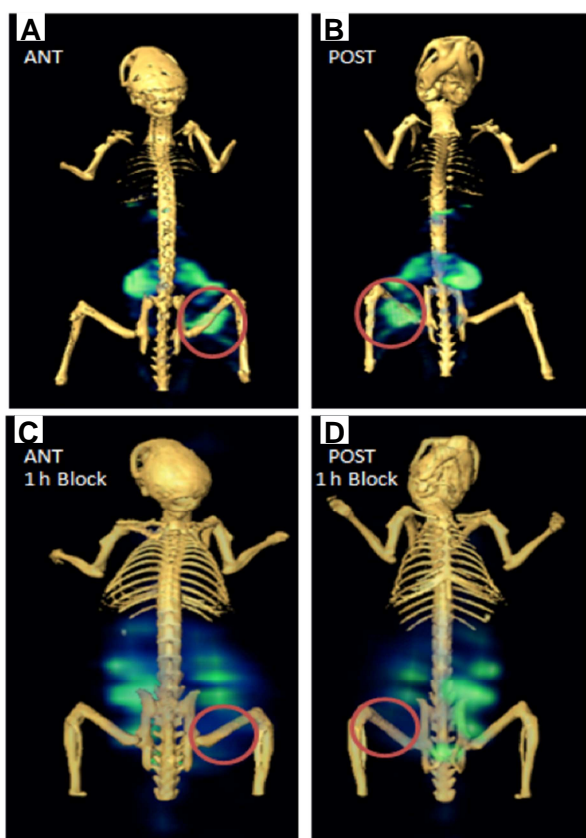
Fig. 5 Athymic nude mice bearing U87MG tumors were scanned (15 min tomography) after the injection of 24.2 MBq with 1 h block using ~300 fold excess of native c(RGDfK) (101.7 µg/kg/mice). **(A & B)** Anterior and posterior scan with remarkable uptake at tumor site. **(C & D)** represent 1 h block with c(RGDfK) clearly showing displacement of the radiotracer from the tumor site.

Biodistribution studies

Biodistribution study of the ^{99m}Tc-DTPA-bis-c(RGDfK) was performed in nude mice bearing B16F10 and U87MG tumors in order to quantify localization of the radiolabeled peptide. U87MG xenografted nude mice were sacrificed and dissected (n = 15, 5 per time interval) at 1, 2, and 4 h p.i. B16F10 xenografted nude mice were sacrificed (n = 10) at 1 h and 2.5 h. The results (Fig. 6) were expressed in percentage of the dose administered per gram of tissue. Each data point represented an average of 5 animals. The main activities were found at the level of the urinary tract in the kidney (7.27 ± 1.16 % ID/g) showing that renal routes mainly excreted the complex. Strong activities were found in spleen (2.55 ± 0.23 % ID/g) and in lungs (2.59 ± 0.41 % ID/g). Soft tissues (muscles) accumulated negligible quantities of the tracer and localization of the radioactivity in the liver and intestine was low (less than 1.0 % ID/g at 2 h post-injection) (Fig. 6).

The radiolabeled peptide displayed high accumulation in the $\alpha_v\beta_3$ positive tumors, U87MG human glioblastoma (5.60 % ID/g versus 0.23 % ID/g for the muscle at 60 min p.i.) and the B16F10 murine melanoma (1.56 % ID/g versus 0.53 % ID/g for the muscle at 150 min p.i., data not shown). Muscles were considered as negative control. The tumor/muscle ratios were 24.35 and 2.92 for U87MG and B16F10 tumors respectively. So, even if tumor binding seemed to be limited for B16F10, the ratio of specific binding compared to the background showed, for each type of tumor, significant values. The specific binding of the ^{99m}Tc-DTPA-bis-c(RGDfK) on U87MG was further supported by the co-injection of the blocking dose of c(RGDfK), where 94.01 ± 2.1 % block was observed. These values indicated both specificity and retention.

Localization of the positive control, U87MG tumor, was possible and murine melanic tumor B16F10 could be readily identified. Moreover, these comparative studies pointed out the predominant renal excretion pathway.

Discussion

Malignant glioma is one of the most aggressive primary brain tumor with poor survival rates and universal recurrence despite aggressive treatments.[11,12]

Melanoma diagnosis is mainly clinical and techniques used for diagnosis and staging lack specificity with relatively high false-positive rate and with a low sensitivity for the detection of occult regional nodal metastases. Early detection is crucial, new tracers have to be developed in order to get an early information and diagnosis.[13–17]
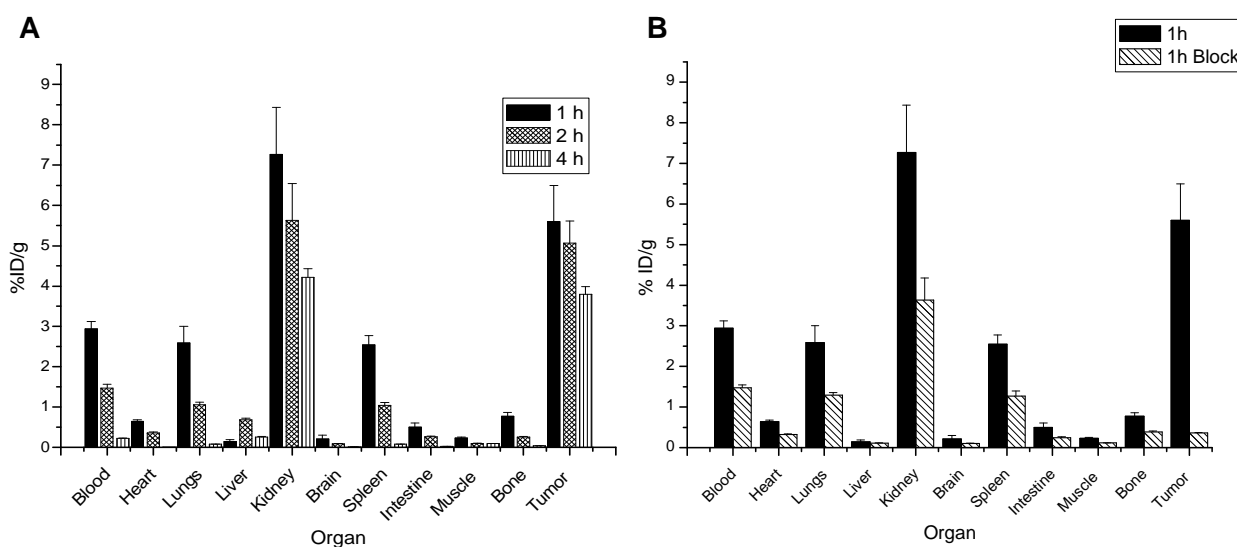
Fig. 6 Biodistribution study in U87MG xenografted mice. **(A)** ^{99m}Tc-DTPA-bis-c(RGDfK) showed mainly renal excretion. Post-injection accumulation 60 min was 7.2 ± 1.16 % ID/g in kidney and 0.14 ± 0.04 % ID/g in liver. **(B)** Comparison of biodistribution with co-injection of blocking dose of c(RGDfK) (101.7 µg/kg/mice) and ^{99m}Tc-DTPA-bis-c(RGDfK). 94.01 ± 2.1 % block was observed.

In this respect, radiolabeled RGD peptides used for non-invasive molecular imaging of $\alpha_v\beta_3$ integrin expression are interesting tools for early detection and treatment of rapidly growing tumors. The concept of bivalency has been applied to develop ^{99m}Tc-DTPA-bis-c(RGDfK), a dimeric RGD peptide, in order to improve tumor targeting compared to the corresponding monomeric RGD peptide analog. The DTPA was chosen for its two potential reactive sites starting from bis-anhydride. In fact, conjugation of RGD peptide is possible *via* the formation of an amide bond between the ε-amine of lysine and the anhydride function. This structure allows also the formation of complex with only one chelate per metal atom, which is required for *in vivo* stability and biological activity. Moreover, ^{99m}Tc-labeled derivatives should be more widely available and clinically applicable.

In vitro binding specificity of DTPA-bis-c(RGDfK) to the $\alpha_v\beta_3$ integrin was demonstrated by the binding inhibition of echistatin to cells and coated receptors. Binding assays gave us value that agreed closely with IC_{50} value of echistatin in the literature and displayed high affinity of our RGD peptide for $\alpha_v\beta_3$ integrin with also excellent Kd values.[18] The results obtained with our tracer were better than those of the positive control c(RGDfK). The binding of echistatin was competed by cyclic RGD peptides whereas no competition was observed with a cyclic peptide containing RAD sequence, confirming the implication of the RGD sequence in the binding of echistatin to $\alpha_v\beta_3$.[19]

Concerning affinity determination of the peptide, different parameters have to be taken into account. First of all, tumor targeting and binding experiments are dependent on the integrin $\alpha_v\beta_3$ quantity on tumor cells, tumor neovasculature and on the binding medium. Some experiments showed higher values for cyclic RGD peptides with entire cell than with purified receptors. So, it's not possible to completely exclude that RGD peptides may non-specifically bind to other integrins.

These experiments depicted high affinity and specificity of our radiotracer for $\alpha_v\beta_3$ integrin. [2,11,18]

To ease the interpretation of the *in vivo* and *in vitro* experiments, $\alpha_v\beta_3$ expression was evaluated in tumor and cells, in order to link our radiolabeling results to the $\alpha_v\beta_3$ expression level of the target. The use of positive or negative control for cells and tissue section experiments demonstrated the specificity or our tracer for $\alpha_v\beta_3$ integrin. Co-localization of the LM609 monoclonal antibody, and [99m]TC-DTPA-bis-c(RGDfK), as well as displacement studies with an excess of cold c(RGDfK), confirmed the specificity of the labeling. To optimize these results, an incubation time of 90 min was chosen for the labeling to get an equilibrium state (Fig. S2 in supplementary information).

Log *P* result was in accordance with the retention time obtained in HPLC and underlined hydrophilic properties but lower than those of the reference, ^{99m}Tc-HYNIC-RGD (log *P* = -3.5).[20]

SPECT images confirmed high uptake in $\alpha_v\beta_3$ receptor positive tumor and low uptake in negative tumor xenografts, thus demonstrating specific receptor mediated uptake *in vivo*. The tumor was clearly visualized by SPECT/CT with good contrast. Then, considering $\alpha_v\beta_3$ expression, it is not surprising to see a high uptake in lungs of tumor bearing mice.[21,22] The high specificity and selectivity of the results in uptake and distribution were confirmed in animal models with and without co-administration of blocking dose.

Because of a wide variety of linkers and chelators for ^{99m}Tc, establishing a comparison among radiolabeled RDG tracers is difficult. Nevertheless, we can notice that tumor uptake of ^{99m}Tc-DTPA-bis-c(RGDfK) is comparable with the results of c(RGDfK)-(Orn)₃-[CGG-^{99m}Tc] (3.32 ± 0.09% ID/g at 30 min p.i.) or of ^{99m}Tc-AuNP-RGD (3.65 ± 0.19% ID/g at 60 min p.i.), and relatively high in comparison to ^{99m}Tc-PGC-c(RGDyK) with tumor uptake of 1.38 ± 0.30% ID/g at 120 min p.i. or [99m]Tc-

DKCK-RGD (1.1% ID/g in melanoma, 2.2% ID/g in osteosarcoma, at 240 min p.i.).[23–26]

As shown by biodistribution studies, radiolabeled cyclic RGD monomers may be useful for imaging integrin $\alpha_v\beta_3$ expression in tumors, but pharmacokinetics optimization is required for clinical utility because of their relatively low tumor uptake and partial hepatobiliary excretion. To improve the $\alpha_v\beta_3$ binding affinity and pharmacokinetics, multimerization has been developed, and different linkers have been incorporated such as sugar moiety to increase excretion *via* the renal pathway.[5,6]

Both small size of the peptide and hydrophilic properties could explain the pharmacokinetics profile of our dimeric peptide. Kidney were mainly concerned for the excretion of ^{99m}Tc-DTPA-bis-c(RGDfK).

Plasma protein binding and lipophilicity varied significantly between different radiolabeled conjugates, leading to considerable differences in pharmacokinetic profiles as well as in tumor uptake (0.2-2.7 %ID/g). Nevertheless, other RGD derivatives, such as ^{99m}Tc-EDDA–HYNIC-RGD, c(RGDfK)-(Orn)$_3$-[CGG-^{99m}Tc], ^{99m}TcO(MAG$_2$-3G$_3$-dimer), or ^{99m}Tc-RAFT-RGD, have presented similar elimination pathway with a main excretion *via* the renal pathway and to a lesser degree the hepatobiliary route.[20,23,27,28]

The fast radiotracer washout observed from normal organs was linked to integrin density. Early imaging was facilitated due to this rapid reduction in background radioactivity. But at later time points, imaging may be improved thanks to further reduction in background noise from the surrounding tissues.[26]
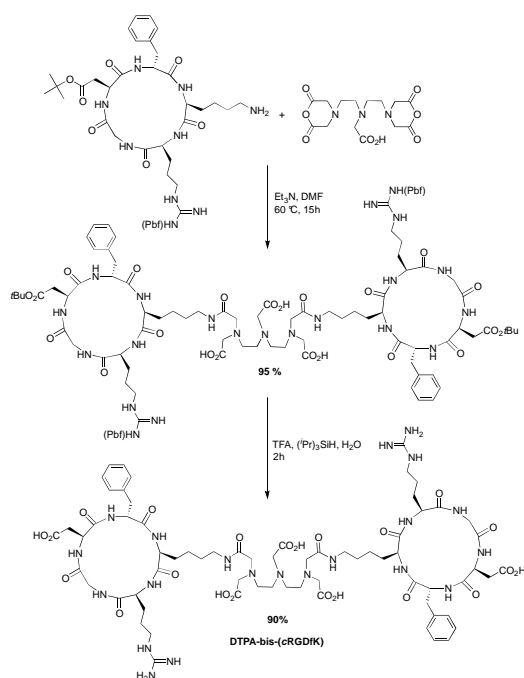
Scheme 1 Synthetic pathway for DTPA-bis-c(RGDfK)

Experimental

Synthesis and purification of DTPA-bis-c(RGDfK)

The linear peptide (RGDfK) was synthesized by solid-phase synthesis onto a Liberty 1 (CEM) microwave peptide synthesizer using a trityl chloride resin (TCP resin, Sigma-Aldrich), applying the standard 9-fluorenylmethyloxycarbonyl (Fmoc) strategy.[29,30] The final Fmoc protecting group was removed with 20% solution of piperidine in DMF. The next steps (cleavage from the resin, cyclization and removal of the Z protecting group) were successfully carried out as described by Haubner *et al.*[30]

The synthesis of DTPA-bis-c(RGDfK) was carried out using the strategy described by Hazari *et al.* (Scheme 1).[31,32] DTPA dianhydride (9 mg, 25 µmol, Sigma-Aldrich) and protected c(RGDfK) (46 mg, 50 µmol) were dissolved in 20 mL of anhydrous DMF. Triethylamine (28 µL, 0.2 mmol, Sigma-Aldrich) was then added and the reaction was allowed to proceed for 15 h at 60 °C. Solvents were removed under reduced pressure and the conjugate was precipitated with diethyl ether. Deprotections of Pbf (2,2,4,6,7-pentamethyldihydrobenzofuran-5-sulfonyl) and *tert*-butyl protecting groups were achieved by treatment of the protected adduct in 20 mL of TFA/(*i*Pr)$_3$SiH/H$_2$O (92/4/4) at room temperature for 2 h. The DTPA-bis-c(RGDfK) conjugate (33 mg, 21 µmol) was then precipitated and washed with cold diethyl ether. Matrix-assisted laser desorption ionization (MALDI) time-of-flight (TOF) mass spectrometry (MS) (Fig. S3 in supplementary information) was performed on a Voyager mass spectrometer (Applied Biosystems) equipped with a pulsed N$_2$ laser (337 nm) and a time-delayed extracted ion source. MALDI-TOF-MS: [M+H]$^+$ = 1564.6 (1564.8 Da calculated for C$_{68}$H$_{102}$N$_{21}$O$_{22}$). HPLC was performed onto the protected DTPA-bis-c(R(Pbf)GD(tBu)fK) and the deprotected DTPA-bis-c(RGDfK) (Fig. S4 and S5 in supplementary information). The column was a Luna C18 (250 mm x 4.6 mm x 5 µm). The flow rate was 1 mL/min with mobile phase starting from NH$_4$OH 50 mM / MeOH (95/5), followed by a linear gradient over 30 min to NH$_4$OH 50 mM / MeOH (5/95).

Solid-phase receptor binding assay

In vitro affinity and specificity of DTPA-bis-c(RGDfK) were assessed *via* binding assays using ^{125}I-Echistatin (Perkin Elmer) as the integrin $\alpha_v\beta_3$ specific radioligand and unlabeled echistatin (Sigma-Aldrich) as reference, by modification of a previously described method.[33] Moreover, c(RGDfK) and c(RADfK) purchased from GeneCust (Dudelange, Luxembourg) were tested as competitor and negative control respectively. Briefly, human integrin $\alpha_v\beta_3$ (Merck Millipore, Darmstadt, Germany) was diluted at 20 ng/mL in coating buffer (20 mM Tris, pH 7.4, 150 mM NaCl, 2 mM CaCl$_2$, 1 mM MgCl$_2$, 1 mM MnCl$_2$). An aliquot of 100 µL/well was added to a Millipore 96-well multiscreen IP filter plates (pore size 0.45 µm) and incubated overnight at 4°C. The plate was washed once with blocking/binding buffer (50 mM Tris, pH 7.4, 100 mM NaCl, 2 mM CaCl$_2$, 1 mM MgCl$_2$, 1 mM MnCl$_2$, 1% bovine serum albumin), and incubated an additional 2 h at room

temperature with 150 µL/well of blocking/binding buffer. The plate was then rinsed twice with the same buffer and incubated for 3 h at room temperature with shaking with ^{125}I-Echistatin (30 pM/well, volume activity 2500 Bq/mL, 500 Bq/well) in presence of increasing concentrations of each competitor (0 – 100 µmol/L). The total volume in each well was adjusted to 200 µL. The plates were filtered through a multiscreen vacuum manifold and unbound radioligand was removed by three additional washes. The filters were collected and the radioactivity was evaluated using a γ-counter (Packard COBRA II, Packard Instruments). Non-specific binding was determined in presence of an excess of echistatin (1000 fold molar excess) and was subtracted from the total binding to yield specific binding. When ^{125}I-ligand incubations were performed without receptor, no interaction was detected due to non-specific adsorption onto the microliter well. Each point was the average of triplicate data points and the results were representative of three experiments. The best-fit 50% inhibitory concentration (IC$_{50}$) values were calculated by fitting inhibition values by non-linear regression using GraphPad Prism (GraphPad Software, Inc.). To confirm the results, binding study was also performed on U87MG cells using increasing concentrations of ^{99m}Tc-DTPA-bis-c(RGDfK) (see supplementary information for experimental procedure).

Immunohistochemical analysis

Different $\alpha_v\beta_3$ positive and negative tumors were formalin-fixed and paraffin-embedded. Immunohistochemical integrin $\alpha_v\beta_3$ detection was performed on serial sections in order to validate radiolabeling analysis. Appropriate positive and negative controls omitting the primary antibody were included with every slide run.

Paraffin embedded 5 µm thick sections were deparaffinized with xylene, rehydrated through a graded alcohol series, and washed with distilled water. A blocking step was needed in order to block endogenous peroxidase activity. After washing with PBS, the slides were saturated with BSA 0.2% in PBS 0.01 M for 30 min, then incubated with the primary antibody (LM609, 1:200) in humidified atmosphere (12 h, 4°C). Sections were washed twice with PBS, and the secondary biotinylated antibody (goat anti-mouse antibody, EnVision[TM] MultiLink, Dako) was applied in moist chamber for 1 hour. Tissue sections were stained with AEC (3-Amino-9-EthylCarbazole, ab 64252, Abcam, Cambridge) for 10 min and counterstained with hematoxylin for examination.

[99m]Tc radiolabeling

DTPA-bis-c(RGDfK) was synthesized in our laboratory and [Na^{+} [99m]TcO$_4$[-]] was obtained from a commercial [99]Mo/^{99m}Tc generator (Elumatic III, IBA international, France).

In a rubber-sealed vial, 1.56 mg (1 µmol) of DTPA-bis-c(RGDfK) was dissolved into 200 µL of water to form a stock solution. Then 50 µL of this solution (390 µg of DTPA-bis-c(RGDfK)) were transferred into a leaded shielded vial along with 100 µl of tin(II) solution in 10 % acetic acid (SnCl$_2$.2H$_2$O, 0.5 mg/mL). 500

µl of [99m]TcO$_4$[-] (360 MBq) were then added and pH was adjusted at 7 by addition of Na$_2$CO$_3$ (0.1 M, 900 µL). This final solution was then heated for 45 min at 95°C.

After cooling, the complex was purified using a C18 Oasis HLB cartridge (Waters, Taunton, USA), preliminarily activated with 5 mL of ethanol and 20 mL of water. The cartridge was loaded with the reaction mixture and then washed with 10 mL of water. The purified tracer was eluted with 2 mL of ethanol. Solvents were removed by heating at 80°C for 5 min and applying a gentle stream of nitrogen. ^{99m}Tc-DTPA-bis-c(RGDfK) (165 MBq) was finally diluted with saline (NaCl 0.9%) for injection.

Radiochemical purity was determined by thin layer radiochromatography (ITLC-SG type sheet, Pall Corporation) using acetone or acetone/NaCl 0.9% (1/1) as eluent. In acetone [99m]TcO$_4$[-] migrated in front of solvent while reduced/hydrolysed ^{99m}Tc and ^{99m}Tc-DTPA-bis-c(RGDfK) did not migrate. On the other hand with acetone/NaCl 0.9% (1/1) the complex migrated with a Rf of 0.9 while ^{99m}Tc colloids remained at the origin. Radiochemical purity was determined after integration of each peak. Radiochemical purity was determined with following formula: 100% - (% of hydrolysed technetium + % of free technetium).

The chemical purity was also checked by analytical HPLC (Luna column C18 (250 mm x 4.6 mm x 5 µm), CH$_3$CN/NH$_4$OH 0.2% (40/60), 0.5 mL/min), R$_t$ = 6.0-6.3 min.

Log *P* values

Log *P* value of ^{99m}Tc-DTPA-bis-c(RGDfK) was determined as described previously.[20] Briefly, ^{99m}Tc-DTPA-bis-c(RGDfK) in PBS was added to 0.5 mL of octanol in an Eppendorf vial. The tube was vigorously vortexed and centrifuged at 5000 x g for 3 min. Aliquot of both aqueous and octanol layers were collected and counted in a γ-counter. Log *P* values were then calculated (log *P* = [(octanol layer activity) / (aqueous layer activity)]).

Radiochemical stability

The stability of the labeled compound was evaluated using ascending thin layer chromatography on ITLC-SG strips and a Raytest miniGITA radiochromatograph (Wilmington USA) using NaCl 0.9%/Acetone (1/1) as eluent. The stability of the radiolabeled conjugate was evaluated at 30, 60, 120 and 180 min at which the percentage of remaining ^{99m}Tc-DTPA-bis-c(RGDfK) was calculated.

Cell cultures

Murine melanoma cell line (B16F10, $\alpha_v\beta_3$ positive) from C57Bl/6 mice (ATCC reference # CRL-6322) were cultured in DMEM medium with 4.5 g of glucose supplemented with 10% FCS, 1% glutamine (GlutaMAX[TM], Invitrogen, Cergy Pontoise, France), 100 UI/mL penicillin and 100 µg/mL streptomycin.

Human melanoma cell line (SKMEL28, $\alpha_v\beta_3$ positive) was obtained from a malignant melanoma of a 51 years old man. Cells were cultured in RPMI 1640 medium supplemented with

10% FCS, 1% glutamine (GlutaMAX^{TM}, Invitrogen, Cergy Pontoise, France), 100 UI/mL penicillin and 100 µg/mL streptomycin.

Human adult glioblastoma cells (U87MG, $\alpha_v\beta_3$ positive) derived from malignant glioma, were cultured in DMEM medium supplemented with 10% FCS, 100 UI/mL penicillin and 100 µg/mL streptomycin.

Rat glioma cell line (C6, $\alpha_v\beta_3$ negative) was cloned from a rat glial tumor induced by N-nitrosomethylurea (ATCC reference # CCL-107). Cells were cultured in DMEM medium supplemented with 5% FCS, 100 UI/mL penicillin and 100 µg/mL streptomycin.

The cells were maintained at 37°C in humidified atmosphere of 5% CO_2 and 95% air. Cells were grown in culture until 80% of confluence. Cells were harvested and suspended in binding buffer (culture medium with 0.1% Bovine Serum Albumin (BSA), Hepes 20 mM pH 7.4).

Time course and kinetics of transport of ^{99m}Tc-DTPA-bis-c(RGDfK)

Cells were incubated with binding buffer for 45 min. This medium was then removed and replaced by 100 µL of cells suspension (100 000 cells/well). Cells were incubated for different times (15 min to 180 min) at 37°C in triplicate with either ^{99m}Tc-labeled peptide in binding buffer (100 µL, volume activity 1 MBq/mL, total series) or 20 µM echistatin and ^{99m}Tc-labeled peptide in binding buffer (100 µL, non-specific series). Incubation was interrupted by aspiration, removal of medium and rapid rinsing twice with ice-cold PBS (200 µL). Furthermore, cell radioactivity was measured with a γ-counter. The results were decay corrected and fitted to 2 million cells by well.

Ex vivo imaging: Radiolabeling of tumor tissue sections

As for immunohistochemical analysis, tumor sections were studied. 5 µm thick slices were deparaffinized and prepared as previously described.

Then, ^{99m}Tc-DTPA-bis-c(RGDfK) was added (296 kBq/40 µL) and slices were incubated at room temperature for 60 min. Unbound radioligand was removed with PBS-Tween 0.05 % and slices were washed in distilled water. Radioactivity was finally evaluated using a micro-imager 2000 (Biospace Lab, Paris). To ensure specific binding, displacement studies were performed using c(RGDfK) (40 µL, 1 mM) which was applied for 90 min after radiolabeled peptide exposure.

In vivo evaluation of radiolabeled peptides

All animal experiments were performed in accordance with the European Community Standards on the Care and Use of Laboratory Animals and approved by the Animal Ethics Committee of our University and also in accordance with the protocol approved by INMAS Institutional Animal Ethics Committee (CPCSEA Regn No.8/GO/a/99). All animals were bred and housed under pathogen free conditions and provided water and food *ad libitum*.

Different type of tumor models were used for the *in vivo* biodistribution and imaging studies. C6 tumor cells were used as negative control and U87MG as positive control of integrin expression.

The cells were centrifuged (5 min, 200 x g) and the pellet was suspended in sterile NaCl 0.9% for extemporaneous administration to the animal.

Tumor uptake studies were performed in female nu/nu mice (Charles River, L'Arbresle, France) and different models were tested: SKMEL28, B16F10, C6, U87MG. Xenografts were subcutaneously injected at a concentration of 2 x 10^6 cells/mouse and allowed to grow until tumors of 150 mm^3 were visible. Tumor bearing mice were used in biodistribution and imaging studies. On the day of the experiment, each mouse was injected with ^{99m}Tc-DTPA-bis-c(RGDfK) (18.5 MBq) intravenously into the tail vein. Blocking experiments were conducted in U87MG implanted tumor in athymic nude mice and performed with a large excess of native c(RGDfK) (101 µg/kg/mice). Mice bearing U87MG tumors were scanned (15 min tomography) after 1 h post injection. Quantitative analysis was done using Amide 1.0.4 software and 3D Image was processed on VIVID (Amira, San diego, USA) software.

SPECT-CT imaging of tumor bearing mice

SPECT was used as it allows high sensitivity sequential measurements in the same animal and quantification on samples. SPECT of tumor bearing mice was performed on a SPECT-CT Symbia$^®$ T2 (GE HealthCare) and in a same manner, SPECT TRIUMPH (GE HealthCare) trimodality system with N5F75A10 multipinhole collimator, mouse style with 1 mm aperture was used to acquire images. Mice were imaged in the prone position. Mice were first anesthetized with intraperitoneal injection of ketamine (100 mg/kg) and xylazine (10 mg/kg). Mice were injected with 18.5 MBq of ^{99m}Tc-DTPA-bis-c(RGDfK) *via* tail vein. Residual activity of the syringe was quantified with activimeter measurement. The tomographic SPECT data acquisition was performed about 30 min after radiotracer injection. For each SPECT scan, regions of interests (ROIs) were drawn over each tumor, normal tissue and major organ and fixing volume were evaluated on FLEX SPECT TM version 1.0.7 in single reconstruction mode OSEM (Ordered Subset Expectation Maximization). The acquisition protocol was composed of 3 tomographies of 10 min associated to scan followed by a 30 min tomography with scan. The final sequence was constituted of 3 tomographies of 10 min each with scan. CT-reconstruction and SPECT-CT images were fused and analyzed with VIVID (Amira, San diego, USA). The mice were sacrificed by cervical dislocation 150 min post-injection. Negative controls were included using C6 xenograft model (murine melanoma model).

Biodistribution studies

We investigated the biodistribution as well as the elimination pathway of ^{99m}Tc-DTPA-bis-c(RGDfK) in mice bearing melanoma or glioma tumors (n = 25). Biodistribution analysis

combined two steps. The first approach used *in vivo* animal scintigraphic imaging in order to check the accumulation of the tracer in the tumor area as well as the main non-specific organs, the distribution and the pharmacokinetics parameters. A quantitative systematic biodistribution study was then performed using organ counting. The mice were sacrificed by cervical dislocation on average at 1, 2 and 4 h post administration.

Tumors and normal tissues (blood, lungs, heart, spleen, liver, bone, kidney, muscle and intestines) were removed from each animal. They were collected, weighed, and the amount of radioactivity was determined using a γ-counter. The percentage of injected dose per gram of tissue (%ID/g) or percentage of injected dose (%ID) was determined for each sample and tumor to organ ratios were calculated.

Statistical analysis

The results were expressed as mean ± standard deviation (SD). Statistical analysis was performed using GraphPad Prism software (version 6.0, La Jolla California USA). Tracer activities and tracer activity ratios were compared using an unpaired t test. A p value ≤0.05 was considered significant.

Conclusions

The objective is now to target intimate mechanisms of oncogenesis and dissemination process of the disease. This option appears of great interest either for aggressiveness detection or for selection of responder to new-targeted therapies. Concerning the structure of the tracer, the dimeric RGD peptide ^{99m}Tc-DTPA-bis-c(RGDfK) showed high *in vitro* integrin affinity and effective *in vivo* tumor targeting. Moreover, technetium is still the most widely available diagnostic radionucleide with optimal physical characteristics for SPECT. Although ^{18}F-labeled or ^{68}Ga-labeled derivatives will be interesting for PET positron emission tomography with advantages in terms of sensitivity and spatial resolution, ^{99m}Tc-derivates would remain the more widely available and clinically applicable.

Acknowledgements

References

1. O. Schnell, B. Krebs, J. Carlsen, I. Miederer, C. Goetz, R. H. Goldbrunner, H. J. Wester, R. Haubner, G. Popperl, M. Holtmannspotter, H. A. Kretzschmar, H. Kessler, J. C. Tonn, M. Schwaiger and A. J. Beer, *Neuro-Oncology*, 2009, **11**, 861–870.
2. J. Folkman, *Nature medicine*, 1995, **1**, 27–31.
3. J. J. Feige, *Bulletin du cancer*, 2010, **97**, 1305–1310.
4. I. Dijkgraaf, A. Y. Rijnders, A. Soede, A. C. Dechesne, G. W. van Esse, A. J. Brouwer, F. H. M. Corstens, O. C. Boerman, D. T. S. Rijkers and R. M. J. Liskamp, *Organic & biomolecular chemistry*, 2007, **5**, 935–944.
5. S. Liu, *Bioconjugate chemistry*, 2009, **20**, 2199–2213.
6. R. H. Haubner, H. J. Wester, W. A. Weber and M. Schwaiger, *The quartely journal of nuclear medicine : official publication of the Italian Association of Nuclear Medicine (AIMN) [and] the International Association of Radiopharmacology (IAR)*, 2003, **47**, 189–199.
7. R. Haubner, H. J. Wester, F. Burkhart, R. Senekowitsch-Schmidtke, W. Weber, S. L. Goodman, H. Kessler and M. Schwaiger, *Journal of nuclear medicine : official publication, Society of Nuclear Medicine*, 2001, **42**, 326–336.
8. X. Chen, R. Park, Y. Hou, V. Khankaldyyan, I. Gonzales-Gomez, M. Tohme, J. R. Bading, W. E. Laug and P. S. Conti, *European journal of nuclear medicine and molecular imaging*, 2004, **31**, 1081–1089.
9. X. Chen, R. Park, A. H. Shahinian, J. R. Bading and P. S. Conti, *Nuclear medicine and biology*, 2004, **31**, 11–19.
10. S. Liu, Z. Liu, K. Chen, Y. Yan, P. Watzlowik, H. J. Wester, F. T. Chin and X. Chen, *Molecular imaging and biology : MIB : the official publication of the Academy of Molecular Imaging*, 2010, **12**, 530–538.
11. R. K. Jain, E. di Tomaso, D. G. Duda, J. S. Loeffler, A. G. Sorensen and T. T. Batchelor, *Nature reviews. Neuroscience*, 2007, **8**, 610–622.
12. P. Y. Wen and S. Kesari, *The New England journal of medicine*, 2008, **359**, 492–507.
13. S. Negrier, P. Saiag, B. Guillot, O. Verola, M. F. Avril, C. Bailly, D. Cupissol, S. Dalac, A. Danino, B. Dreno, J.-J. Grob, M. T. Leccia, C. Renaud-Vilmer, L. Bosquet, *Bulletin du cancer*, 2006, **93**, 371–384.
14. C. M. Balch, J. E. Gershenwald, S. J. Soong, J. F. Thompson, M. B. Atkins, D. R. Byrd, A. C. Buzaid, A. J. Cochran, D. G. Coit, S. Ding, A. M. Eggermont, K. T. Flaherty, P. A. Gimotty, J. M. Kirkwood, K. M. McMasters, M. C. Mihm, D. L. Morton, M. I. Ross, A. J. Sober and V. K. Sondak, *Journal of clinical oncology : official journal of the American Society of Clinical Oncology*, 2009, **27**, 6199–6206.
15. P. Queirolo and M. Acquati, *Cancer treatment reviews*, 2006, **32**, 524–531.
16. C. Garbe, K. Peris, A. Hauschild, P. Saiag, M. Middleton, A. Spatz, J. J. Grob, J. Malvehy, J. Newton-Bishop, A. Stratigos, H. Pehamberger, A. M. Eggermont, *European journal of cancer (Oxford, England : 1990)*, 2012, **48**, 2375–2390.
17. C. K. Bichakjian, A. C. Halpern, T. M. Johnson, A. Foote Hood, J. M. Grichnik, S. M. Swetter, H. Tsao, V. H. Barbosa, T. Y. Chuang, M. Duvic, V. C. Ho, A. J. Sober, K. R. Beutner, R. Bhushan, and W. Smith Begolka, *Journal of the American Academy of Dermatology*, 2011, **65**, 1032–1047.
18. C. C. Kumar, H. Nie, C. P. Rogers, M. Malkowski, E. Maxwell, J. J. Catino and L. Armstrong, *The Journal of pharmacology and experimental therapeutics*, 1997, **283**, 843–853.
19. J. E. Fisher, M. P. Caulfield, M. Sato, H. A. Quartuccio, R. J. Gould, V. M. Garsky, G. A. Rodan and M. Rosenblatt, *Endocrinology*, 1993, **132**, 1411–1413.

20 C. Decristoforo, B. Faintuch-Linkowski, A. Rey, E. von Guggenberg, M. Rupprich, I. Hernandez-Gonzales, T. Rodrigo and R. Haubner, *Nuclear medicine and biology*, 2006, **33**, 945–952.

21 R. Haubner, B. Kuhnast, C. Mang, W. A. Weber, H. Kessler, H. J. Wester and M. Schwaiger, *Bioconjugate chemistry*, 2004, **15**, 61–69.

22 B. Singh, C. Fu and J. Bhattacharya, *American journal of physiology. Lung cellular and molecular physiology*, 2000, **278**, L217–226.

23 I. Tsiapa, G. Loudos, A. Varvarigou, E. Fragogeorgi, D. Psimadas, T. Tsotakos, S. Xanthopoulos, D. Mihailidis, P. Bouziotis, G. C. Nikiforidis and G. C. Kagadis, *Nuclear medicine and biology,* 2013, **40**, 262–272.

24 E. Morales-Avila, G. Ferro-Flores, B. E. Ocampo-Garcia, L. M. De Leon-Rodriguez, C. L. Santos-Cuevas, R. Garcia-Becerra, L. A. Medina and L. Gomez-Olivan, *Bioconjugate chemistry*, 2011, **22**, 913–922.

25 D.-E. Lee, Y.-D. Hong, K.-H. Choi, S.-Y. Lee, P.-H. Park and S.-J. Choi, *Applied radiation and isotopes : including data, instrumentation and methods for use in agriculture, industry and medicine*, 2010, **68**, 1896–1902.

26 R. Haubner, F. Bruchertseifer, M. Bock, H. Kessler, M. Schwaiger and H. J. Wester, *Nuklearmedizin. Nuclear medicine*, 2004, **43**, 26–32.

27 J. Shi, L. Wang, Y. S. Kim, S. Zhai, B. Jia, F. Wang and S. Liu, *European journal of nuclear medicine and molecular imaging*, 2009, **36**, 1874–1884.

28 L. Sancey, V. Ardisson, L. M. Riou, M. Ahmadi, D. Marti-Batlle, D. Boturyn, P. Dumy, D. Fagret, C. Ghezzi and J. P. Vuillez, *European journal of nuclear medicine and molecular imaging*, 2007, **34**, 2037–2047.

29 G. B. Fields and R. L. Noble, *International journal of peptide and protein research*, 1990, **35**, 161–214.

30 R. Haubner, H. J. Wester, U. Reuning, R. Senekowitsch-Schmidtke, B. Diefenbach, H. Kessler, G. Stocklin and M. Schwaiger, *Journal of nuclear medicine : official publication, Society of Nuclear Medicine*, 1999, **40**, 1061–1071.

31 P. P. Hazari, G. Shukla, V. Goel, K. Chuttani, N. Kumar, R. Sharma and A. K. Mishra, *Bioconjugate chemistry*, 2010, **21**, 229–239.

32 S. K. Sethi, R. Varshney, S. Rangaswamy, N. Chadha, P. P. Hazari, A. Kaul, K. Chuttani, M. D. Milton and A. K. Mishra, *RSC Adv.*, 2014, **4**, 50153-50162.

33 R. A. Orlando and D. A. Cheresh, The *Journal of biological chemistry*, 1991, **266**, 19543–19550.

RSC Advances Accepted Manuscript